E. Polydorou et al., Adv. Mater. Interfaces 4, 1700231 (2017)

Improved Stability of Polymer Solar Cells in Ambient Air *via* Atomic Layer Deposition of Ultra-Thin Dielectric Layers

*Ermioni Polydorou, Martha A. Botzakaki, Ilias Sakellis, Anastasia Soultati, Andreas Kaltzoglou, Theodoros A. Papadopoulos, Joe Briscoe, Charalabos Drivas, Kostas Seintis, Mihalis Fakis, Leonidas C. Palilis, Stavroula N. Georga, Christoforos A. Krontiras, Stella Kennou, Polycarpos Falaras, Nikos Boukos, Dimitris Davazoglou, Panagiotis Argitis, Maria Vasilopoulou**

Dedicated to Prof. Michael L. Hitchman

E. Polydorou, Dr. A. Soultati, Dr. A. Kaltzoglou, Dr. P. Falaras, Dr. N. Boukos, Dr. D. Davazoglou, Dr. P. Argitis, Dr. M. Vasilopoulou
Institute of Nanoscience and Nanotechnology, National Center for Scientific Research Demokritos, 15310, Agia Paraskevi, Attiki, Greece
*m.vasilopoulou@inn.demokritos.gr

Dr. I. Sakellis
Institute of Nanoscience and Nanotechnology, National Center for Scientific Research Demokritos, 15310, Agia Paraskevi, Attiki, Greece
University of Athens, Physics Department, Section of Solid State Physics, Panepistimioupolis, 15684 Zografos, Athens, Greece

Dr. M. A. Botzakaki, K. Seintis, Prof. M. Fakis, Prof. L. C. Palilis, Prof. S. N. Georga, Prof. C. A. Krontiras
Department of Physics, University of Patras, 26504 Patras, Greece

Dr. T. A. Papadopoulos
Department of Natural Sciences, University of Chester, Thornton Science Park, CH2 4NU, Chester, U. K.

Dr. Joe Briscoe
Materials Research Institute, School of Engineering and Materials Science, Queen Mary University of London, U. K.

C. Drivas, Prof. S. Kennou
Department of Chemical Engineering, University of Patras, 26504 Patras, Greece

Keywords: Atomic layer deposition, polymer solar cells, stability, passivation, ZnO.

Polymer solar cells have attracted tremendous interest in the highly competitive solar energy sector, due to the practical advantages they exhibit, such as being lightweight, flexible and low cost, in stark contrast to what traditional photovoltaic technologies offer. However, their successful commercialization is still hindered by issues related to device instability. Here, we employ atomic layer deposition (ALD) to deposit conformal ultra-thin dielectrics, such as alumina (Al_2O_3) and zirconia (ZrO_2), on top of ZnO films to address problems arising from the defect-rich nature of these films and demonstrate improved characteristics when they are used as electron extraction materials. The deposition of dielectrics on ZnO significantly improved its interfacial electronic properties, manifested primarily with the decrease of the work function of ZnO and the concomitant reduction of the electron extraction barrier as well as reduced recombination losses. Significant efficiency enhancement was obtained with the incorporation of 6 ALD cycles of Al_2O_3 into inverted devices, using photoactive layers, that consist of poly(3-hexylthiophene) (P3HT):indene-C_{60} bisadduct ($IC_{60}BA$) or poly({4,8-bis[(2-ethylhexyl)oxy]benzo[1,2-b:4,5-b′]dithiophene-2,6-diyl}{3-fluoro-2-[(2-ethylhexyl)carbonyl] thieno[3,4-b] thiophenediyl}) (PTB7):[6,6]-phenyl C70 butyric acid methyl ester ($PC_{70}BM$). More importantly, upon performing lifetime studies (over a period of 350 h) a strong improvement in polymer solar cell stability was observed in the ALD-modified ZnO-films.

1. Introduction

Polymer solar cells (PSCs), based on polymer donors and fullerene acceptors, have gained significant attention as an alternative photovoltaic technology due to their flexibility, low-cost and roll-to-roll manufacturing.[1-2] Presently, PSCs based on interpenetrating donor:acceptor networks exhibit power conversion efficiencies (PCEs) exceeding 10% for single-junction[3,4] and 12% for tandem-junction devices consisting of stacks of individual cells with complementary absorption spectra.[5,6] However, the technology is still under development in the key area of device stability. The implementation of inverted architectures has significantly improved the stability over that of the convention architectures.[7] Moreover, with the insertion of functional interfacial layers, i.e. an electron extraction layer (EEL) and hole extraction layer (HEL), between the electrodes and the photoactive film, the stability and overall performance of the PSCs could be further increased.[8-10]

Amongst solution processed interfacial materials, metal oxides with intrinsic n-type conductivity, such as zinc oxide (ZnO), have been considered as promising candidates for EELs due to their inherent transparency, tunable electronic properties, low toxicity and facile thin-film preparation through a diverse range of solution-processing techniques.[11-15] However, surface defects of ZnO that act as electron trapping sites and moisture and oxygen species adsorbed therein that have been proven to be corrosive agents strongly degrade solar cell performance and have a negative impact on the cell stability.[16-21] Therefore, the development of processes for effective passivation of ZnO against oxygen, moisture and its surface defects is of vital importance in order to enhance the device stability. Furthermore, work function modification of ZnO may also promote the longevity of the cells. Several efforts have been made to simultaneously circumvent the surface defect and adsorbate-induced degradation, and control the work function (W_F) of ZnO. Some effective approaches proposed so far include employing self-assembled monolayers (SAMs), small molecules or high-molar-mass polymers such as poly(ethylene oxide) (PEO) and poly(ethylene glycol) (PEG) and non-conjugated polymers at the interfaces between the photoactive layers and ZnO.[22-28] Development of doped ZnO-based materials with a variety of different dopants, such as aluminum, indium, cesium, nitrogen and hydrogen, has also been shown to improve the efficiency and stability of the fabricated cells.[29-34]

On the other hand, atomic layer deposition (ALD) of dielectric oxides has been established as a viable and effective approach for the surface passivation of several metal oxides (including ZnO) in order to improve their optoelectronic properties,[35,36] and it has also been implemented in silicon solar cell technology.[37] Recently, ALD dielectric oxides have been considered as promising candidates for reducing undesirable surface recombination in dye-sensitized and perovskite solar cells.[38-45] In addition, ALD-Al_2O_3 was used as an EEL in PSCs with conventional architecture,[46] while our group introduced the use of ultra-thin ALD Al_2O_3 and ZrO_2 layers to passivate surface defects of TiO_2 for improving efficiency in PSCs with inverted architecture.[47]

In the current work, we successfully apply an ultrathin (<1nm) layer of Al_2O_3 and ZrO_2 by ALD on the surface of ZnO EELs to significantly increase both the efficiency and the stability under ambient air of intentionally un-encapsulated inverted PSCs. With the incorporation of 6 ALD cycles of Al_2O_3 into devices using photoactive layers consisting of either P3HT:$IC_{60}BA$ or PTB7:$PC_{70}BM$, the PCEs of these cells significantly increased to 6.75 and 8.23%, respectively. The results represent an improvement of 30-35% as compared to the reference cells without the ALD coatings. The efficiency enhancement stemmed from the synergistic effects of surface defect passivation, lowering of the work function of ZnO, facilitated electron transport and reduced recombination losses at the cathode interface after the incorporation of the dielectric coatings. More significantly, while intentionally un-encapsulated devices based on un-passivated ZnO showed moderate environmental stability, those using ALD coating passivated EELs exhibited prolonged lifetimes under ambient air maintaining 81% for P3HT:$IC_{60}BA$-based devices and 74% for PTB7:$PC_{70}BM$-based ones of the initial PCE values after 350 hours of operation. The enhanced stability is attributed to partial passivation of the oxide surface upon ALD-dielectric coating preventing molecular oxygen.

2. Results and discussion

2.1 Experimental and theoretical investigation of the passivation effect of ALD dielectrics coated on ZnO layers. ZnO films were spin-coated on FTO (on glass) substrates from a zinc acetate precursor and

then annealed in air at 250 ºC for 20 minutes. These films exhibited a compact and pin-hole free surface morphology (Figure S1, Supporting Information) and a hexagonal wurtzite crystalline phase (Figure S2). Ultra-thin Al_2O_3 and ZrO_2 layers were applied on ZnO films using 6 ALD deposition cycles. Their nominal thickness is about 5.5 Å, according to the estimated deposition rate of 0.94 Å/cycle (as provided by the manufacturer). The chemical composition of these dielectric layers on ZnO was verified by X-ray photoelectron spectroscopy (XPS) (Figure S3). The estimated average thickness of the deposited layers by XPS, after taking into account the presence of an approximately 6.0 Å thick layer of adventitious C on top, was found to be around 3.0 Å for both layers.[48] We expect that this disagreement in thickness might be due to the presence of pinholes in the films. Note that, both ALD layers were amorphous.[49]

The role of ALD dielectrics as passivation layers on ZnO was first explored by using photoluminescence (PL) measurements (Figure S4). The significant decrease of the broad visible emission peak of ZnO after deposition of the ALD dielectrics (especially of alumina) implies partial surface passivation of the ZnO.[50,51] Furthermore, Density Functional Theory (DFT) calculations also predicted the passivation effect of Al_2O_3 and ZrO_2 on the ZnO_x (0002) surface. In our previous work, we demonstrated the formation of gap states on the O-terminated ZnO (0002) surface was attributed to unsaturated O atoms.[52] Since oxygen vacancies have the lowest formation energy among the surface defects of ZnO that behave as electron donors, we incorporated in our model their formation prior to the creation of the interface; the ZnO_x (0002) surface, where x=0.87, was then constructed and optimized. One quarter of the surface oxygen atoms were removed from the slab (**Figure 1a**, left panel) providing an O-vacancy coverage density of $\rho = 2.73 \cdot 10^{14}$ cm^{-2}. **Figure 1b** shows the density of states (DOS) of the O-terminated ZnO_x (0002) surface; the presence of states located at -0.19 eV and in a range between -2.05 and -1.50 eV below the Fermi level, consist of O 2*p* and hybridized 2*d* orbitals with nearly no contribution from Zn states is observed (Figure S5). Next, we constructed and optimized the Al_2O_3/ZnO_x and ZrO_2/ZnO_x interfaces (**Figure 1a**, middle and right panel). Our calculations indicate that this process releases -7.73 eV of energy per Al_2O_3 and -2.03 eV of energy per ZrO_2 adsorbent unit. In terms of both interfaces, the calculated DOS (**Figure 1c** and **Figure 1d**, respectively) shows a strong suppression of the surface oxygen states, observed below the Fermi level for the pristine ZnO_x (0002) surface (Figure 1b). After calculating the band decomposed charge density in the range ~0.3 eV above the Valence Band Maximum (VBM), we observe that oxygen *p* and hybridized *d* orbitals are relocated to the VBM (Figure S6, S7 and S8). According to Bader charge analysis performed at both interfaces,[53] charge transfer occurs from the ALD oxides to the ZnO_x (0002) surface oxygen atoms, at a maximum of ~0.93 |e| and ~0.19 |e| for the ZnO_x/Al_2O_3 and ZnO_x/ZrO_2 interface respectively, which is mainly responsible for the shift of the gap states towards the VBM. Our calculations indicate that passivation of the ZnO_x surface may occur via charge transfer from the ALD oxide to ZnO_x surface oxygen atoms which is more pronounced in the case of Al_2O_3.

Since the work function of ZnO plays a crucial role in the charge extraction process and overall device performance, we next performed ultraviolet photoemission spectroscopy (UPS) measurements on the samples. **Figure 1e** shows the UPS spectra of ZnO before and after the ALD deposition of 6 cycles for both Al_2O_3 and ZrO_2. As seen in Figure 1e, the un-passivated ZnO exhibits a work function of 4.1(±0.1) eV. Notably, the work function was reduced to 3.8(±0.1) eV upon deposition of ALD-dielectrics. This decrease in the work function may result in an electron extraction barrier lowering, thus facilitatingelectron transport and extraction from the photoactive film to the ZnO layer. A decrease in the intensity of the UPS spectrum around 5 eV is observed upon deposition of the ALD-oxides. This could be due to hydrogen incorporation within the ZnO lattice in the form of interstitial dopants (i.e., bonded to oxygen), as also indicated by the fourier transform infra-red (FTIR) spectra recorded on un-passivated and dielectric-coated ZnO films (with a thickness of 500 nm, Figure S9). These H dopants come from the ALD deposition environment since one of the precursors for the growth of both dielectric oxides is water. Note that our group has recently shown that H dopants also act as passivation agents, since they are able to terminate dangling bonds present at the oxide's bulk and surface.[54] Furthermore, the position of the valence band edge with respect to the surface Fermi level was determined by extrapolating the leading edge of the valence band photoemission spectra to the intersection with the background level to account for the finite resolution of the spectrometer. It is observed that the ZnO valence band edge shifts towards higher binding energies i.e. (higher energy difference from the valence band edge to the Fermi level) by about 0.3 eV (from 3.3 to 3.6 eV) upon deposition of the ALD-dielectrics. This behavior is in agreement with results from the literature and

indicates a downward shift of the valence band maximum due to the passivation effect of ALD-dielectrics.[55] The ionization energy is found to be 7.4 eV for both un-passivated and passivated ZnO films. The conduction band minimum, which was calculated from UPS measurements and the optical bandgap of the ZnO film (Figure S10), was found to be 4.1eV. This implies that the valence and conduction bands of ZnO shift towards lower energies upon deposition of ALD-dielectrics. Furthermore, a similar (0.3 eV) downward vacuum level shift as a result of an interfacial dipole is also observed at the ALD-modified ZnO interface.

2.2 Solar cell performance enhancement via ALD-dielectric deposition on ZnO layers. Having established the pivotal role of ALD-dielectric for the surface passivation of the ZnO layers we next employed the passivated ZnO films as EELs in PSCs adopting the inverted architecture, illustrated in **Figure 2a**; the chemical structures of the semiconducting polymers and fullerenes used in this study are also shown. In **Figure 2b,** the energy diagram of the layer sequence used at the cathode side of the device is illustrated. It is shown that upon ALD deposition the work function of ZnO decreases by 0.3 eV as a result of the formation of a negative interfacial dipole (with its negative pole pointing towards the ZnO surface). This decreases the electron extraction barrier and strengthens the built-in voltage (**Figure 2c**). Both effects should facilitate charge separation and electron extraction and result in faster electron transport towards the cathode, which is beneficial for the overall device performance.

The effect of ALD layer thickness on the device performance was first investigated by fabricating a series of P3HT:$IC_{60}BA$-based solar cells with ZnO films either un-passivated or ALD-coated with an increasing number of ALD cycles (2, 4, 6, 8 and 10 cycles) (Figure S11). It was found that devices incorporating ALD layers obtained with 2-6 deposition cycles exhibited considerable improvement in all photovoltaic performance parameters as compared with the reference device, which exhibits a short-circuit current density (J_{sc}) of 10.2 mA cm^{-2}, an open-circuit voltage (V_{oc}) of 0.77 V and a fill factor (FF) of 0.64 yielding a PCE of 5.03% (**Figure 3a** and **Table 1**). PSCs obtained using 6 cycles of ALD –dielectrics were the best performing (and most stable, as discussed below) with a J_{sc} of 11.30 and 11.60 mA cm^{-2}, V_{oc} of 0.80 and 0.82 V and FF of 0.69 and 0.71, yielding PCEs of 6.24 and 6.75% for ZrO_2 and Al_2O_3 coating, respectively. The efficiencies of the passivated cells are therefore 24% and 34% higher compared with the reference device. Note that control samples in which the ZnO is treated for the same time, at the same temperature (250 ºC), and water dosing conditions, but without the oxide precursors, exhibited performance nearly similar to that of the reference cell. The comparatively more pronounced efficiency enhancement in the Al_2O_3-modified devices may result from more surface effective passivation of ZnO. This is because passivation upon deposition of ALD-dielectrics proceeds through charge transfer from the dielectric oxide (having a high density of fixed negative charges) to ZnO. This reduces the depletion layer width at the surface of ZnO caused by adsorbed negatively charged oxygen species and induces downward band bending (referred to as "field-effect passivation").[56,57] Charge transfer is more pronounced in the case of Al_2O_3 (as also predicted by theoretical calculations presented above) probably due to its well-known ability to contain a very high density of fixed negative charges.[58-60] In addition, the dark J-V characteristics (shown in **Figure 3b** on semi-logarithmic scale) are greatly improved in the case of ALD-modified devices with respect to the reference ones. This suggests that the ALD-coating reduces reverse leakage and shunt current, enhances the rectification ratio and minimizes interfacial recombination as a result of surface defects passivation and subsequent reduction of the interfacial trap density. In addition, it facilitates electron injection and/or transport, thus enhancing J_{sc}, as a result of increasing the built-in voltage (**Figure 2c**). Both reduction of the reverse saturation current and increase of the built-in voltage contribute to the increase of the V_{oc} observed in the ALD-modified cells. The large improvement in J_{sc} can also be verified by external quantum efficiency (EQE) measurements (**Figure 3c**). Notably, the incorporation of ZnO films coated with ALD-dielectrics significantly enhanced the efficiency without affecting the spectral shape of the EQE.

To demonstrate the general use of the proposed ALD modification approach for improved PSCs applications, we also applied ZnO films coated with ALD-dielectrics in another efficient polymer:fullerene-PSC system. We chose PTB7:$PC_{70}BM$ photoactive blends and found that the device performance was also improved upon ALD deposition of ultra-thin conformally-coated ZrO_2 and Al_2O_3 films on ZnO (**Figures 3d**). The significant improvement in FF, J_{sc} and V_{oc} of the cells with the ALD modified films yielded PCEs of 7.72% and 8.23% in ZnO/ZrO_2 and ZnO/Al_2O_3 based devices, representing a 24.3 and 32.5% enhancement

in comparison with the reference cell (PCE of 6.21%). A higher rectification ratios (lower leakage current) (**Figure 3e**) and an improved photon-to-electron conversion efficiency (**Figure 3f**) were also observed in the cells with ALD-modified ZnO films. Again, optimal performance was obtained in the devices using Al_2O_3-coated ZnO layers, which is attributed to the more effective surface passivation of ZnO, as compared to ZrO_2-coated ZnO layers.

To investigate whether there are morphological reasons for the performance enhancement of the ALD-dielectric oxide modified PSCs, we also probed the surface topography of ZnO before and after coating with ALD-dielectrics. As shown in the atomic force microscopy (AFM) surface topographies (Figure S12), there are some differences in the surface morphology of ZnO layers before and after the ALD coating. However, these small deviations in surface morphology could not explain the significant difference in device efficiency. In addition, it is unclear from AFM if the ALD-dielectrics are pinhole free. We expect that pin-holes must exist in those films because the XPS estimated thickness of 3.0 Å is different than the nominal one (5.5 Å). In the case that pinholes are indeed present even at 5% of the surface area, they may act as point-contacts where unimpeded charge transfer is funneled through.[61,62] This could result in reduced surface recombination as well as increased shunt resistance and, therefore, in an enhancement of the solar cell performance as observed in ALD-modified devices. Interestingly, the spreading of the active layer dichlorobenzed-based solutions was excellent for all surfaces of samples prepared in this work, verifying the effective wetting of the ALD-dielectrics with the photoactive overlayers, despite the higher contact angles (lower hydrophilicities) measured in the ALD-coated ZnO layers (Figure S13). Consequently, there were only minor differences in surface nanomorphology of the photoactive blends (of P3HT:$IC_{60}BA$, in particular) deposited on different ZnO substrates as evidenced by AFM topographies presented in Figure S14. These surface topography investigations suggest that, upon deposition of ALD-dielectrics on ZnO, there is small alteration of the morphology of the photoactive blend.

2.3 Improved stability of ALD modified solar cells. In addition to efficiency, the ambient stability of polymer solar cells is of great importance.[63] In view of the role of ALD-dielectrics as protective layers against ambient air induced degradation, an aging study of the devices was performed. The photovoltaic parameters of PSCs acquired during the course of the aging study are depicted in **Figure 4**. Note that the devices were intentionally un-encapsulated so that they were exposed to ambient conditions (moisture and oxygen) throughout the aging study. The J-V measurements of a batch of five identical cells of each kind were performed at room temperature in ambient air and the devices were kept in the dark in between successive measurements. The variation of PCE over aging time (where error bars are included to allow for tests of statistical significance), J_{sc}, V_{oc} and FF for P3HT:$IC_{60}BA$ and PTB7:$PC_{70}BM$-based devices using ZnO (**Figure 4a** and **Figure 4d**), ZnO/ZrO_2 (**Figure 4b** and **Figure 4e**) and ZnO/Al_2O_3 (**Figure 4c** and **Figure 4f**) layers implies significant stability improvement in the ALD-modified devices. Continuing our study up to 350 hours, we observed that the ALD-dielectrics significantly delay the air-induced degradation thereby retaining about 74% and 81% of their initial PCE, for ZnO/ZrO_2 and ZnO/Al_2O_3, respectively, while the pristine devices retained only 43% of their initial PCE. The remarkable stability of our un-encapsulated cells is comparable or even exceeds previously reported values for PSCs based on P3HT with a fullerene acceptor.[64]

Fascinatingly, the same conclusion can be drawn from stability measurements taken on devices based on PTB7. Due to the long and easily cleavable alkoxy side chains in the polymer backbone, PTB7:$PC_{70}BM$-based devices are highly susceptible to oxygen and moisture induced degradation when compared to P3HT:$IC_{60}BA$-based devices. Therefore, the reference PTB7:$PC_{70}BM$-based cells were significantly degraded when exposed to air retaining only 29% of their initial PCE after 350 hours. After ZnO was coated with ALD-dielectric oxides, the PCE decreases to about 65% of the initial values for ZnO/ZrO_2 and 70% for ZnO/Al_2O_3, manifesting the vast potential of our ALD design for stable, scalable solar cells with practical shelf and operating lifetimes.[65]

The enhanced stability of our devices can be partly explained by the fact that ALD-Al_2O_3 films can form very effective gas barriers thus preventing adsorption of oxygen and moisture (which oxidize and corrode the photoactive blends) on the ZnO surface.[66-68] In addition, during the ALD deposition the already adsorbed water molecules participate in reactions with trimethylaluminum or tetrakis (dimethylamide) zirconium precursors to form the first monolayers of Al_2O_3 or ZrO_2 and, therefore, are no longer available to

act as corrosion agents at the surface of ZnO. Note that, 6-10 cycles of ALD deposition seem to be the optimum range in terms of device stability. For 2 and 4 cycles of ALD deposition, the stability results are sub-optimal. This may be due to incomplete coverage of ZnO with the ALD-dielectric so that the initial exposure to air still has a dominant deleterious effect. Increasing the number of cycles beyond 10 cycles, on the other hand, significantly deteriorates the J_{sc} and the FF (results not shown), perhaps due to inadequate charge tunneling through the ALD-dielectric.

2.4 Additional solar cell characterization. Effective surface passivation of ZnO upon ALD deposition is also expected to reduce interfacial recombination. This is verified from the variation of V_{oc} of P3HT:$IC_{60}BA$ (**Figure 5a**) and PTB7:$PC_{70}BM$ (**Figure 5b**) based devices illuminated with different light intensities. It is shown that both types of reference devices exhibit slopes of V_{oc} versus the natural logarithm of the light intensity larger than KT/q (1.89 KT/q and 1.42 KT/q, respectively), thus indicating a strong dependence on light intensity when using the un-passivated ZnO EELs. This can be attributed to a large density of trapping sites and a concomitant large increase in the number of Shockley-Read-Hall (SRH) (monomolecular) or trap assisted recombination processes in the reference cells.[69] In contrast, the slopes obtained in the ZnO/ZrO_2-based devices are significantly lower (1.26 and 1.11 KT/q for P3HT:$IC_{60}BA$ and PTB7:$PC_{70}BM$, respectively), whereas those of the ZnO/Al_2O_3-based devices are even lower approaching 1.0 KT/q (in particular, 1.12 and 1.04 KT/q, respectively). This indicates a much slower surface recombination rate and enhancement of selectivity of the cathode contact approaching conditions where bimolecular (e.g. Langevin) recombination dominates. The presence of the ALD-dielectrics reduced the number of trapping sites that act as recombination centers by passivating surface defects on ZnO and lowering the energy barrier between the photoactive layer and the modified cathode, leading to enhanced FF and PCE values.

The better selectivity of the cathode was further verified by J-V measurements taken in electron-only devices with the following structure: FTO/ZnO/photoactive layer/Al (**Figure 5c** and **Figure 5d**), where the MoO_x/Al hole selective contact is replaced with Al, which is able to inject electrons into the lowest unoccupied molecular orbital (LUMO) of fullerene acceptors. It is evident that for low operation voltages both devices based on ZnO show relatively small current densities in the forward direction, while a substantial increase in electron current is found in the ALD-modified ZnO devices. This indicates a reduction of the electron extraction barrier and better selectivity of the cathode contact, leading to enhanced J_{sc} values.

2.5 Photophysical properties of photoactive polymers on zinc oxides. Time resolved photoluminescence (TRPL) measurements were next taken on P3HT films deposited on ZnO samples to elucidate the charge separation and recombination dynamics at the ZnO/P3HT interfaces. Two different thickness P3HT layers , prepared using 3.0 mg/mL (**Figure 6a**) and 1.5 mg/ml ortho-dichlorobenzene solutions (**Figure 6b**), were coated on the ZnO samples for TRPL measurements to enable a more thorough study on the interfacial charge transfer from P3HT to ZnO. The 468 nm nanosecond laser source was used to directly excite P3HT films coated on ZnO and therefore, the acquired TRPL signals detected at 720 nm directly reflect the fluorescence decay of P3HT. The fluorescence lifetime (τ) of each sample was estimated by fitting the TRPL semi-log decay curves using a three-exponential function. The extracted parameters are reported in Tables S1 and S2. It is observed that the ZnO/P3HT and ZnO/ALD-dielectric/P3HT exhibited similar average lifetime (0.25 ns for un-passivated ZnO, 0.27 ns for ZnO/ZrO_2 and 0.24 ns for ZnO/Al_2O_3, for the 20 nm thick P3HT and 0.21 ns/0.23ns/0.21 ns for the 10 nm thick P3HT). These results do not agree with those previously reported by our group where considerably increased fluorescence lifetimes of P3HT on ALD-dielectric passivated on TiO_2 were obtained.[47] This increase was attributed to effective passivation of deep lying surface defect states on TiO_2, which act as recombination centers for holes thus reducing hole trapping and increasing the effective exciton lifetime. However, this previous study cannot provide sufficient explanation for our current findings where nearly equal exciton lifetimes were observed in all cases. To explain the trend observed for the fluorescence decay of P3HT on ALD-modified and pristineZnO substrates, we propose that it may be governed by opposing charge separation and recombination processes, in particular, hole trapping and electron transfer that may antagonistically determine P3HT exciton dissociation and decay.[70,71] Passivation of ZnO, except suppressing charge trapping sites which act as hole recombination centers, significantly decreases its work function (which was not observed in TiO_2). This has

the net result of reducing the energy offset between the LUMO of P3HT and the conduction band of ALD-modified ZnO. This effect enables more efficient electron collection and promotes fast, energetically downhill, electron transfer at the ZnO/ALD-dielectric/P3HT interfaces, therefore, reducing the exciton lifetime, as reported also in the literature.[34,72] Identically, the simultaneous suppression of defect-induced hole trapping and enhancement of electron transfer in ALD-coated ZnO granted minor deviations in exciton lifetimes of 40 nm thick PTB7 films deposited on ZnO substrates; this was estimated from TRPL measurements for excitation at 468 nm and detection at 790 nm (**Figure 6c**, Table S3) and 830 nm (**Figure 6d**, Table S4). In particular, the estimated exciton lifetimes of PTB7 deposited on ZnO (0.36ns at 790 nm and 0.37 ns at 830 nm) and ZnO/ZrO_2 (0.35ns/0.36ns) were nearly identical. However, a small increase was obtained when PTB7 was deposited on ZnO/Al_2O_3 substrate (0.40ns/0.43nm). This indicates that the suppression of hole trapping via effective passivation of defect states is more pronounced in the case of alumina (as discussed above) and dominates over the decrease of the electron transfer barrier at the ZnO/Al_2O_3/P3HT interface that would otherwise promote faster exciton dissociation. Notably, steady-state PL measurements (Figure S15) verified that charge separation occurring at the ZnO/Al_2O_3/P3HT interfaces represents a phenomenon predominantly governed by the suppression of the intrinsic deep defects in ZnO.[34] Finally, all findings in this study explicitly confirm the potential of ALD architecture in regulating the ZnO properties and defect states and verify the significance of ALD-controlled interface engineering in photovoltaic and other optoelectronic applications.

3. Conclusions

An ultrathin ALD-dielectric layer was inserted between the ZnO EEL and the photoactive layer of PSCs in order to successfully address the defect-rich nature of ZnO and enhance the efficiency and lifetime of the devices under ambient air. The passivation effect of ALD-dielectrics on ZnO offered a highly controllable platform for improving the selectivity of the modified cathode interface by reducing the electron extraction barrier and suppressing surface recombination. An increase of 30-35% in the PCE of P3HT:$IC_{60}BA$ and PTB7:$PC_{70}BM$-based solar cells was obtained when using ZnO EELs passivated via the application of ALD deposition 6 cycles of Al_2O_3. Moreover, the un-encapsulated ALD-modified devices exhibited a remarkable stability against ambient air retaining 70-80% of their initial PCEs after storage in the dark for 350 hours. This work paves the way for a simple and efficient route towards efficient and stable PSCs manufacturing, and provides important guidelines for the implementation of ALD-dielectrics layers in other contemporary cell architectures.

4. Experimental section

Preparation of ZnO and ALD dielectric layers. ZnO films with a thickness of 50 nm were prepared following a sol-gel method using zinc acetate in 2-methoxyethanol:2-amino-ethanol as a precursor solution with a concentration of 0.50 M. The solution was kept under stirring for 2-3 h at 60ºC using a magnetic stirrer to obtain a homogeneous solution. Next, it was filtered through a 0.45 μm pore size nylon membrane and then spin-coated at 3000 rpm and post-annealed at 250 ºC for 20 min. Zinc acetate was purchased from Sigma-Aldrich and used without further purification. Al_2O_3 and ZrO_2 were deposited using ALD (Savannah-100 ALD system by Cambridge-Nanotech/ USA).[73] Both depositions were performed at 250 °C. The precursors used for the deposition of Al_2O_3 and ZrO_2 were trimethylaluminum (TMA-$Al_2(CH_3)_6$) and tetrakis (dimethylamide) zirconium ($Zr(NMe_2)_4$), respectively, while H_2O was used as the oxidant/co-reactant.

Device Fabrication. Inverted polymer solar cells were fabricated on fluorinated tin oxide (FTO) coated glass substrates which were purchased from Sigma-Aldrich and served as the cathode electrode. Substrates were ultrasonically cleaned with a standard solvent regiment (15 min each in acetone, isopropanol and deionized water). The ZnO layer was then deposited followed by deposition of the photoactive layer. The active layer consisted of P3HT (purchased from Sigma-Aldrich):$IC_{60}BA$ (purchased from Ossila) (17 mg ml^{-1} for P3HT, 17 mg ml^{-1} for $IC_{60}BA$ in 1,2-dichlorobenzene) or of PTB7(purchased from Ossila):$PC_{70}BM$ (purchased from Ossila) (10 mg ml^{-1} for PTB7, 15 mg ml^{-1} for $PC_{70}BM$ in 970 μl of 1,2-dichlorobenzene and 30 μl of 1,8-diiodooctane (DIO)). Solutions were stirred at 65-70 ºC for about 3 hours. P3HT:$IC_{60}BA$ was spin-

coated at 800 rpm for 30 sec to deliver a thickness of 200 nm while the thickness of PTB7:$PC_{70}BM$ was about 90 nm. After spin coating, the photoactive layers were left to dry for about 30 min and then P3HT:$IC_{60}BA$ films were annealed at 150 °C for 10 min while PTB7:$PC_{70}BM$ were not subjected to any post-annealing treatment. Note that all depositions and thermal treatments of photoactive layers were carried out in the inert environment of an argon filled glove box with oxygen and humidity levels below 1.0 ppm. Then, an approximately 30 nm thick under-stoichiometric molybdenum oxide (MoO_x) layer was deposited on top of the photoactive layer to serve as the hole extraction layer.[74] The devices were completed with a 150 nm thick aluminium anode, deposited in a dedicated thermal evaporator at a pressure of 10^{-6} Torr through a shadow-mask, which defined the device active area to be equal to 12.56 mm^2. The devices were then measured in air at room temperature without additional encapsulation.

Measurements and Instrumentation. X-ray photoelectron spectra (XPS) and Ultraviolet Photoelectron Spectra (UPS) were recorded by Leybold EA-11 electron analyzer operating in constant energy mode at pass energy of 100 eV and at a constant retard ratio of 4 eV for XPS and UPS respectively. All binding energies were referred to the C 1s peak at 284.8 eV of surface adventitious carbon. The X-ray source for all measurements was a nonmonochromatized Al Kα line at 1486.6 eV (12 keV with 20 mA anode current). The valence band spectra of ZnO samples were evaluated after recording the UPS spectra of about 50 nm thick films deposited on FTO substrates. For the UPS measurements, the He I (21.22 eV) excitation line was used. A negative bias of 12.22 V was applied to the samples during UPS measurements in order to separate secondary electrons originating from sample and spectrometer and to estimate the absolute work function value from the high BE cut-off region of the UPS spectra. The analyzer resolution is determined from the width of the Au Fermi edge to be 0.16 eV. Photoluminescence measurements on ZnO were carried out using a Horiba Jobin-Yvon iHR320 Spectrometer with a He-Cd laser (325 nm) as excitation source. The steady state photoluminescence spectra of P3HT on various substrates were taken by means of a Fluoromax spectrometer (Horiba) upon excitation at 550 nm. The films were placed on a specific holder for solid samples and the spectra were corrected for the sensitivity of the detector. The PL dynamics of the samples were studied under magic angle conditions, by using a Time Correlated Single Photon Counting (TCSPC) technique Fluotime 200, (Picoquant). The excitation of the samples was realized by means of a ps diode laser at 468 nm having a pulse duration of 80 ps. The fluorescence of the samples was collected and passed through a detection analyzer and a monochromator. It was finally detected by a micro-channel plate photomultiplier. The IRF of the TCSPC spectrometer was ~80 ps. The best fitting was achieved by a multi-exponential function convoluted with the IRF and was determined by inspection of the residuals and through the χ^2 factor which should be smaller than 1.1. EQE measurements were carried out using an Autolab PGSTAT-30 potentiostat, with a 300 W Xe lamp in combination with an Oriel 1/8 monochromator for dispersing the light in an area of 0.5 cm^2. A Thorlabs silicon photodiode was used for the calibration of the spectra. All measurements were performed in air. X-ray diffraction (XRD) structural analysis was performed using a Siemens D500 diffractometer with Cu-K*a* radiation. Absorption measurements were taken using a Perkin Elmer Lambda 40 UV/Vis spectrophotometer. FTIR transmission spectra of ZnO films were obtained on a Bruker Tensor 27 spectrometer (at 4 cm^{-1} resolution, 64 scans) with a DTGS detector. The thicknesses of films were measured with an Ambios XP-2 profilometer and a M2000 Woolam ellipsometer. Current density-voltage characteristics of the fabricated solar cells were measured with a Keithley 2400 source-measure unit. Cells were illuminated with a Xe lamp and an AM 1.5G filter to simulate solar light illumination conditions with an intensity of 100 mW/cm^2 (1 sun), as was recorded with a calibrated silicon photodiode. To accurately define the active area of all devices we used aperture masks during the measurements with their area equal to those of the Al contacts (12.56 mm^2).

Computational Methodology. All theoretical calculations were carried out using the Vienna Ab Initio Simulation Package (VASP). Plane-wave basis sets and the Perdew-Burke-Ernzerhof (PBE) gradient-corrected exchange-correlation functional was used throughout the computational part. We incorporated an effective Hubbard U parameter equal to 8.5 eV as implemented and tested by Li et al.[75] All calculations were performed via the projector augmented wave (PAW) method with a plane-wave cut-off energy of 400 eV and a Γ centered k-point grid of 8×8×1. The tetrahedron method with Blöchl corrections of a width of 0.2 eV was used to determine how partial occupancies are set for each wave function. The ZnO surface slab

was constructed after PBE+U ion optimization, excluding volume, was performed on bulk ZnO at its crystallographic coordinates; these were taken from work done by Kisi et al.[76] The ZnO (0002) surface, which according to Siao et al.,[77] is the most stable and exposed crystal surface of ZnO in the O- and H-rich limits, was modeled using 20 Zn and 24 O atoms within an orthorhombic cell of dimensions a = 6.50 Å, b = 5.63 Å and c = 40 Å. All surface cells were separated by a vacuum space of ~30 Å along z-axis. Geometry optimization, with maximum atomic forces of 0.01 $e \cdot Å^{-1}$ was carried out for the top two ZnO layers emulating surface relaxation, while the bottom three layers were kept fixed at their crystallographic coordinates representing "bulk" ZnO. After the stoichiometric surface of ZnO (0002) was optimized, one surface oxygen atom was manually removed in order to construct the ZnO_x (0002) surface, with x=0.87, corresponding to a slab of 20 Zn and 23 O atoms. Relaxation was then reinitiated and the under-stoichiometric surface was re-optimized following the same procedure.

Supporting Information

Supporting Information is available from the Wiley Online Library or from the author.

Acknowledgements

This work was performed in the framework of "YDISE" project within GSRT's KRIPIS action, funded by Greece and the European Regional Development Fund of the European Union under NSRF 2007–2013 and the Regional Operational Program of Attica. TP acknowledges use of local computational facilities provided by the Faculty of Science and Engineering, University of Chester, U.K.

References

[1] G. Yu, J. Gao, J. C. Hummelen, F. Wudl, A. J. Heeger, *Science* **1995**, *270*, 1789.
[2] S. Mathew, A. Yella, P. Gao, R. Humphry-Baker, B. F. E. Curchod, N. Ashari-Astani, I. Tavernelli, U. Rothlisberger, Md. Khaja Nazeeruddin, M. Grätzel, *Nat. Chem.* **2014**, *6*, 242.
[3] Z. He, B. Xiao, F. Liu, H. Wu, Y. Yang, S. Xiao, C. Wang, T. P. Russell, Y. Cao, *Nat. Photon.* **2015**, *9*, 174.
[4] J.-D Chen, C. Cui, Y.-Q. Li, L. Zhou, Q.-D. Ou, C. Li, Y. Li, J.-X. Tang, *Adv. Mater.* **2015**, *11*, 1035.
[5] Z. Yin, J. Wei, Q. Zheng, *Adv. Sci.* **2016**, *8*, 1500362.
[6] N. Li, D. Baran, G. D. Spyropoulos, H. Zhang, S. Berny, M. Turbiez, T. Ameri, F. C. Krebs, C. J. Brabec, *Adv. Energy Mater.* **2014**, *4*, 1400084.
[7] M. T. Loyd, D. C. Olson, P. Lu, E. Fang, D. L. Moore, M. S. White, M. O. Reese, D. S. Ginley, J. W. P. Hsu, *J. Mater. Chem.* **2009**, *19*, 7638.
[8] M. Vasilopoulou, A. M Douvas, D. G Georgiadou, V. Constantoudis, D. Davazoglou, S. Kennou, L. C Palilis, D. Daphnomili, A. G Coutsolelos, P. Argitis, *Nano Research* **2014**, *5*, 679.
[9] C. K. Song, A. C. White, L. Zeng, B. J. Leever, M. D. Clark, J. D. Emery, S. J. Lou, A. Timalsina, L. X. Chen, M. J. Bedzyk, T. J. Marks, *ACS Appl. Mater. Interfaces* **2013**, *5*, 9224.
[10] A. Ghobadi, T. G. Ulusoy, R. Garifullin, M. O. Guler, A. K. Okyay, *Sci. Rep.* **2016**, *6*, 30587.
[11] J. You, C.-C. Chen, L. Dou, S. Murase, H.-S. Duan, S. Hawks, T. Xu, H. J. Son, L. Yu, G. Li, Y. Yang, *Adv. Mater.* **2012**, *24*, 5267.
[12] R. M. Hewlett, M. A. McLachlan, *Adv. Mater.* **2016**, *28*, 3893.
[13] S. Trost, T. Becker, K. Zilberberg, A. Behrendt, A. Polywka, R. Heiderhoff, P. Görrn, T. Riedl, Sci. Rep. **2014**, *5*, 7765.
[14] J. Gilot, M. M. Wienk, R. A. J. Janssen, *Appl. Phys. Lett.* **2007**, *90*, 143512.
[15] H. Zhang, T. Stubhan, N. Li, M. Turbiez, G. J. Matt, T. Ameri, C. J. Brabec, *J. Mater. Chem.* A **2014**, *2*, 18917.
[16] A. Janotti, C. G. Van de Walle, *Appl. Phys. Lett.* **2005**, *87*, 122102.
[17] K. H. Tam, C. K. Cheung, Y. H. Leung, A. B. Djurišić, C. C. Ling, C. D. Beling, S. Fung, W. M. Kwok, W. K. Chan, D. L. Phillips, L. Ding, W. K. Ge, *J. Phys. Chem. B* **2006**, *110*, 18917.
[18] M. Hartel, S. Chen, B. Swerdlow, H.-Y. Hsu, J. Manders, K. Schanze, F. So, *ACS Appl. Mater. Interfaces* **2013**, *5*, 7215.
[19] Y. Jin, J. Wang, B. Sun, J. C. Blakesley, N. C. Greenham, *Nano Lett.* **2008**, *8*, 1649.

[20] B. A. MacLeod, B. J. T. de Villers, P. Schulz, P. F. Ndione, H. Kim, A. J. Giordano, K. Zhu, S. R. Marder, S. Graham, J. J. Berry, A. Kahn, D. C. Olson, *Energy Environ. Sci.* **2015**, *8*, 592.
[21] M. Prosa, M. Tessarolo, M. Bolognesi, O. Margeat, D. Gedefaw, M. Gaceur, C. Videlot Ackermann, M. R. Andersson, M. Muccini, M. Seri, J. Ackermann, *ACS Appl. Mater. Interfaces* **2016**, *8*, 1635.
[22] K. H. Tam, C. K. Cheung, Y. H. Leung, A. B. Djurišić, C. C. Ling, C. D. Beling, S. Fung, W. M. Kwok, W. K. Chan, D. L. Phillips, L. Ding, W. K. Ge, *J. Phys. Chem. B* **2006**, *110*, 18917.
[23] M. Hartel, S. Chen, B. Swerdlow, H.-Y. Hsu, J. Manders, K. Schanze, F. So, *ACS Appl. Mater. Interfaces* **2013**, *5*, 7215.
[24] S. Bai, Y. Jin, X. Liang, Z. Ye, Z. Wu, B. Sun, Z. Ma, Z. Tang, J. Wang, U. Würfel, F. Gao, F. Zhang, *Adv. Energy Mater*. **2015**, *5*, 1401606.
[25] J. J. Intemann, K. Yao, Y.-X. Li, H.-L. Yip, Y. X. Xu, P.-W. Liang, C.-C. Chueh, F.-Z. Ding, X. Yang, X. Li, Y. Chen, A. K.-Y. Jen, *Adv. Funct. Mater.* **2013**, *24*, 1465.
[26] I. Lange, S. Reiter, M. Pätzel, A. Zykov, A. Nefedov, J. Hildebrandt, S. Hecht, S. Kowarik, C. Wöll, G. Heimel, D. Neher, *Adv. Funct. Mater.* **2014**, *24*, 7014.
[27] S. Bai, Y. Jin, X. Liang, Z. Ye, Z. Wu, B. Sun, Z. Ma, Z. Tang, J. Wang, U. Würfel, F. Gao, F. Zhang, *Adv. Energy Mater.* **2015**, *5*, 1401606.
[28] W. Lee, S. Jeong, C. Lee, G. Han, C. Cho, J.-Y. Lee, B. J. Kim, *Adv. Energy Mater* **2017**, 1602812.
[29] X. Liu,X. Li, Y. Li,C. Song,L. Zhu,W.Zhang, H.-Q.Wang, J. Fang, *Adv. Mater.* **2016**, *28*, 7405.
[30] A. Puetz, T. Stubhan, M. Reinhard, O. Loesch, E. Hammarberg, S. Wolf, C. Feldmann, H. Kalt, A. Colsmann, U. Lemmer, *Sol. Energy Mater. Sol. Cells* **2011**, *95*, 579.
[31] A. Savva, S. A. Choulis, *Appl. Phys. Lett.* **2013**, *102*, 233301.
[32] H. Woo Choi, K.-S. Lee, N. David Theodore, T. L. Alford, *Sol. Ener. Mater. Sol. Cells* **2013**, *117*, 273.
[33] K. P. Musselman, S. Albert-Seifried, R. L. Z. Hoye, A. Sadhanala, D. Muñoz-Rojas, J. L. MacManus-Driscoll, R. H. Friend, *Adv. Funct. Mater.* **2014**, *24*, 3562.
[34] V. Papamakarios, E. Polydorou, A. Soultati, N. Droseros, D. Tsikritzis, A. M. Douvas, L. Palilis, M. Fakis, S. Kennou, P. Argitis, M. Vasilopoulou, *ACS Appl. Mater. Interfaces* **2016**, *8* (2), 1194.
[35] A. Illiberi, Illiberi, R. Scherpenborg, M. Theelen, P. Poodt, F. Roozeboom, *JVST-A* **2013**, *31*, 061504.
[36] J-P Richters, T Voss, D S Kim, R Scholz, M Zacharias, *Nanotechnology* **2008**, *19*, 305202.
[37] G. Dingemans, W. M. M. Kessels, *J. Vac. Technol.* A **2012**, *30*, 040802.
[38] C. Prasittichai, J. T. Hupp, *J. Phys. Chem. Lett.* **2010**, *1*, 1611.
[39] T. W. Hamann, O. K. Farha, J. T. Hupp, *J. Phys. Chem. C* **2008**, *112*, 19756.
[40] T. C. Li, M. S. Góes, F. Fabregat-Santiago, J. Bisquert, P. R. Bueno, C. Prasittichai, J. T. Hupp, T. J. Marks, *J. Phys. Chem. C* **2009**, *113*, 18385.
[41] Z. Lin, C. Jiang, C. Zhu, J. Zhang, *ACS Appl. Mater. Interfaces* **2013**, *5*, 713 .
[42] A. K. Chandiran, P. Comte, R. Humphry-Baker, F. Kessler, C. Yi, M. K. Nazeeruddin, M. Grätzel, *Adv. Funct. Mater.* **2013**, *23*, 2775.
[43] G. Niu, W. Li, F. Meng, L. Wang, H. Dong, Y. Qiu, *J. Mater. Chem. A* **2014**, *2*, 705.
[44] D. Koushik, J. J. H. Verhees, Y. Kuang, S. Veenstra, D. Zhang, M. A. Verheijen, M. Creatore, R. E. I. Schropp, *Energy Environ. Sci.* **2017**, DOI: 10.1039/C6EE02687G.
[45] C. Fei, J. Tian, Y. Wang, X. Liu, L. Lv, Z. Zhao, G. Cao, *Nano Energy* **2014**, *10*, 353.
[46] L. Qi, C. Zhang, Q. Chen, *Thin solid films* **2014**, *567*, 1.
[47] M. Vasilopoulou, D. G. Georgiadou, A. Soultati, N. Boukos, S. Gardelis, L. C. Palilis, M. Fakis, G. Skoulatakis, S. Kennou, M. Botzakaki, S. Georga, C. A. Krontiras, F. Auras , D. Fattakhova-Rohlfing, T. Bein, T. A. Papadopoulos, D. Davazoglou, P. Argitis, *Adv. Energ. Mater.* **2014**, *4*, 1400214.
[48] S. Ladas, L.Sygellou, S. Kennou, M.Wolf, G. Roeder, A.Nutsch, M.Rambach, W.Lerch, *Thin solid Films,* **2011,** 520, 871
[49] M. A. Botzakaki, A. Kerasidou, L. Sygellou, V. Ioannou-Sougleridis, N. Xanthopoulos, S. Kennou, S. Ladas, N. Z. Vouroutzis, Th. Speliotis, D. Skarlatos, *ECS Solid State Lett.* **2012**, *1(2)*, 32.
[50] V. Roge, A. Georgantzopoulou, K. Mehennaoui, I. Fechete, F. Garin, A. Dinia, A. C. Gutleb, D. Lenoble, *RSC Avd.* **2015**, *5*, 97635.

[51] V. Roge, N. Bahlawane, G. Lamblin, I. Fechete, F. Garin, A. D, D. Lenoble, *J. Mater. Chem. A* **2015**, *3*, 11453.
[52] E. E. Polydorou, A. Zeniou, D. Tsikritzis, A. Soultati, I. Sakellis, S. Gardelis, T. A. Papadopoulos, J. Briscoe, L. C. Palilis, S. Kennou, E. Gogolides, P. Argitis, D. Davazoglou, M. Vasilopoulou, *J. Mater. Chem. A* **2016**, *4*, 11844.
[53] W. Tang, E. Sanville, G. Henkelman, *J. Phys.: Condens. Matter* **2009**, *21*, 084204.
[54] E. Polydorou, I. Sakellis, A. Soultati, A. Kaltzoglou, T. Papadopoulos, J. Briscoe, D. Tsikritzis, M. Fakis, L. C. Palilis, S. Kennou, P. Argitis, P. Falaras, D. Davazoglou, M. Vasilopoulou, *Nano Energy* **2017**, *34*, 500.
[55] D. C. Gleason-Rohrer, B. S. Brunschwig, N. S. Lewis, *J. Phys. Chem. C* **2013**, *117*, 18031.
[56] K. Matsunaga, T. Tanaka, T. Yamamoto, Y. Ikuhara, Phys. Rev. B **2003**, *68*, 085110.
[57] N. M. Terlinden, G. Dingemans, M. C. M. Van de Sanden, W. M. M. Kessels, *Appl. Phys. Lett*. **2010**, *96*, 112101 .
[58] B. Hoex, J. J. H. Gielis, M. C. M. van de Sanden, W.M.M. Kessels, *J. Appl. Phys.* **2008**, *104*, 113703.
[59] B. Hoex, J. Schmidt, R. Bock, P.P. Altermatt, M.C.M. van de Sanden, W.M.M. Kessels, *Appl. Phys. Lett.* **2007**, *91*, 112107.
[60] J. Benick, B. Hoex, M. C. M. van de Sanden, W. M. M. Kessels, O. Schultz, S. W. Glunz, *Appl. Phys. Lett.* **2008**, 92 (25), 253504.
[61] B. Vermang, V. Fjällström, J. Pettersson, P. Salomé, M. Edoff, *Solar Energy Materials Solar Cells* **2013**, *117*, 505.
[62] E. Schneiderlöchner, R. Preu, R. Lüdemann, S. W. Glunz, *Progress in Photovoltaics: Research & Applications* **2002**, *10*, 29.
[63] S. M. George, *Chem. Rev.* **2010**, *110*, 111.
[64] P. Cheng, X. Zhan, *Chem Soc Rev* **2016**, *45* (9), 2544.
[65] S. Holliday, R. S. Ashraf, A. Wadsworth, D. Baran., S. A. Yousaf, C. B. Nielsen, C.-H. Tan, S. D. Dimitrov, Z. Shang, N. Gasparini, M. Alamoudi, F. Laquai, C. J. Brabec, A. Salleo, J. R. Durrant, I. McCulloch, *Nat. Comm*. **2016**, *7*:11585, DOI: 10.1038/ncomms11585.
[66] F. J. Lim, A. Krishnamoorthy, G. W. Ho, *ACS Appl. Mater. Interfaces* **2015**, *7* (22), 12119.
[67] M. Li, D. Gao, S. Li, Z. Zhou, J. Zou, H. Tao, L. Wang, M. Xu, J. Peng, *RSC Adv.* **2015**, *5*, 104613.
[68] Z. Ding, J. Kettle, M. Horie, S. W. Chang, G. C. Smith, A. I. Shames, E. A. Katz, *J. Mater. Chem. A* **2016**, *4*, 7274.
[69] J. Reinhardt, M. Grein, C. Buhler, M. Schubert, U. Wurfel, *Adv. Energy Mater*. **2014**, *5*, 1400081.
[70] R. T. Ginting, C. C. Yap, M. Yahaya, M. Mat Salleh, *J. Alloys Compd.* **2014**, *585***,** 696.
[71] Y.-Y. Lin, C.-W. Chen, T.-H. Chu, W.-F. Su, C.-C. Lin, C.-H. Ku, J.-J. Wu, C.-H. Chen, *J. Mater. Chem.* **2007**, *17*, 4571.
[72] H. B. Lee, R. T. Ginting, S. T. Tan, C. H. Tan, A. Alshanableh, H. F. Oleiwi, C. Chin Yap, M. H. Hj. Jumali, M. Yahaya, *Scientific Reports* **2016** , *6*:32645, DOI: 10.1038/srep32645.
[73] A. Kerasidou, M. Botzakaki, N. Xanthopoulos, S. Kennou, S. Ladas, S. N. Georga, C. A. Krontiras, *J. Vac. Sci. Technol. A* **2013**, *31*, 01A126.
[74] I. Kostis, N. Vourdas, G. Papadimitropoulos, A. Douvas, M. Vasilopoulou, N. Boukos, D. Davazoglou, *J. of Phys. Chem. C* **2013**, *117*, 18013.
[75] H. Li, L. K. Schirrar, J. Shim, H. Cheun, B. Kippelen, O. L. A. Monti, L.-L. Brédas, *Chem. Mater.*, 2012, **24**, 3044.
[76] E. H. Kisi, M. M. Elcombe, *Acta Crystallogr., Sect. C: Struct. Commun.* **1989**, *45*, 1867.
[77] Siao, Y.-J., P.-L. Liu, and Y.-T. Wu, *Applied Physics Express* **2011**, *4*(12), 125601.

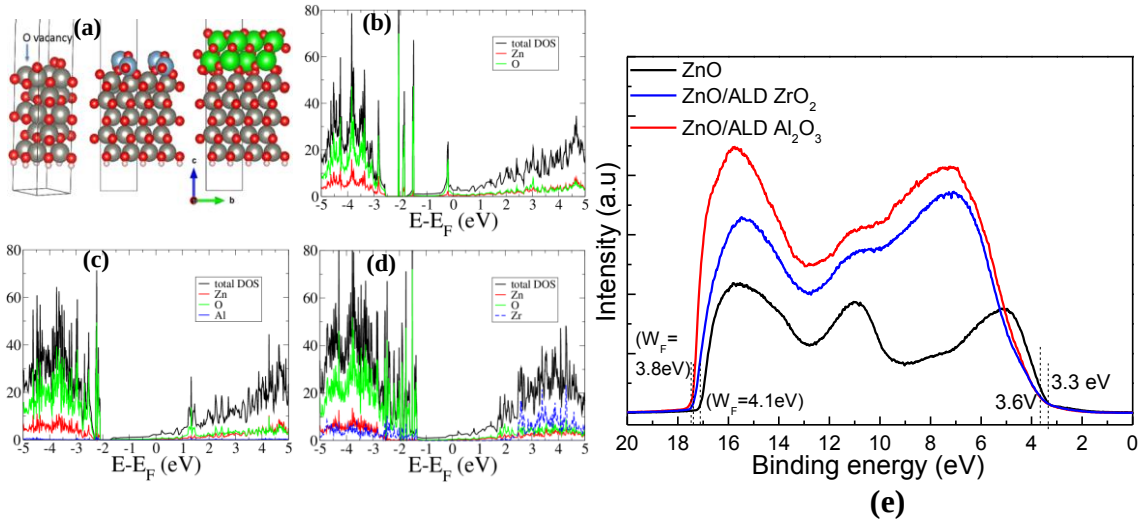

Figure 1 (a) The atomic structure of the ZnO_x bare surface (left), ZnO_x/Al_2O_3 (middle), and ZnO_x/ZrO_2 (right) interfaces. The density of states of (b) the ZnO_x (0002) surface, where x=0.87, (c) the ZnO_x(0002)/Al_2O_3 interface and (d) the ZnO_x(0002)/ZrO_2 interface. (e) UPS spectra of 50 nm thick ZnO films (on glass/FTO substrates), un-passivated and coated with 6 cycles of ALD-dielectrics (Al_2O_3 and ZrO_2).

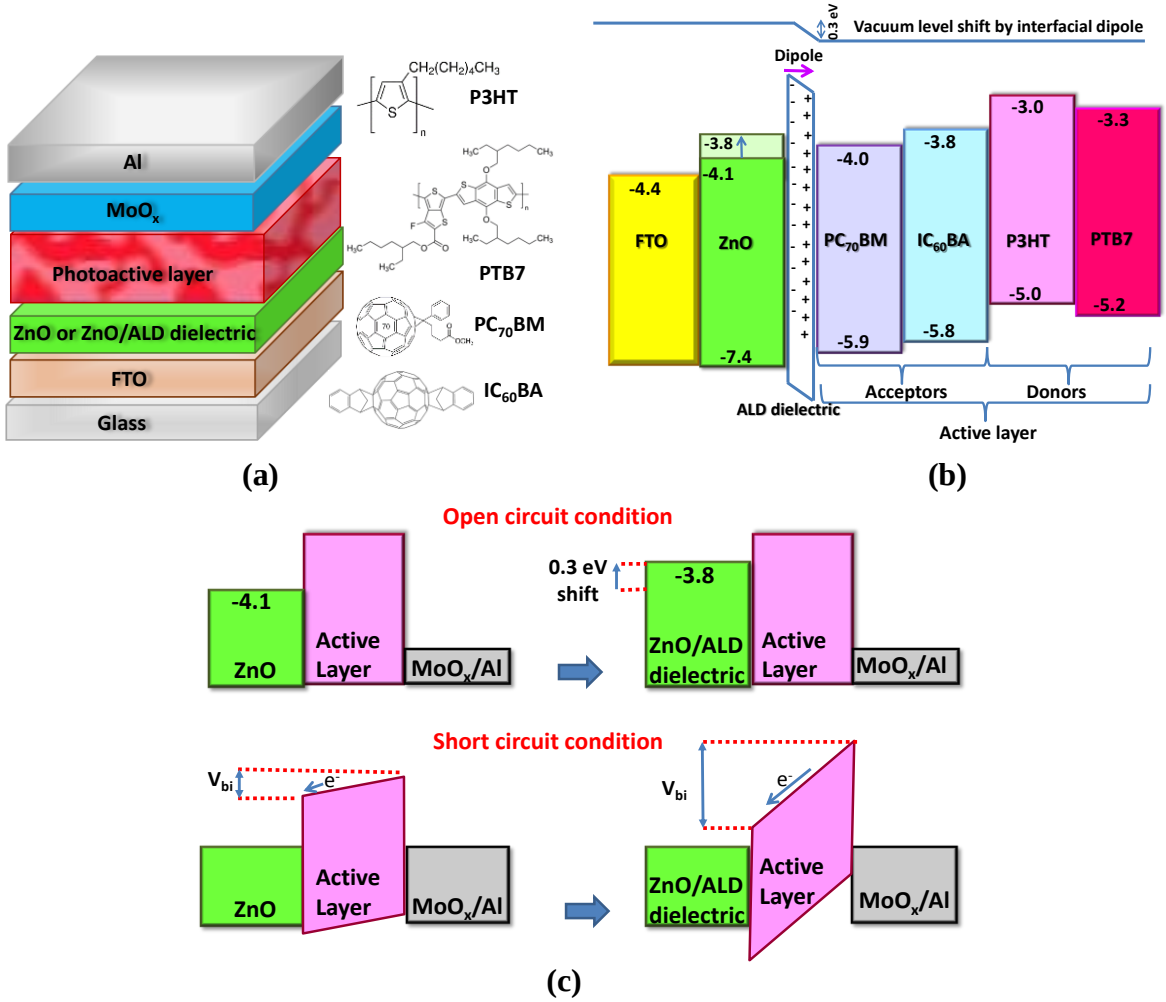

Figure 2 (a) The inverted device architecture and the chemical structures of the organic semiconductors used in this study. (b) Energy band diagram for the materials employed in the devices with un-passivated and ALD-dielectric coated ZnO layer. (c) Energy band diagram at the polymer:fullerene/electrode interfaces under open circuit conditions (upper panel) and short circuit conditions (bottom panel).

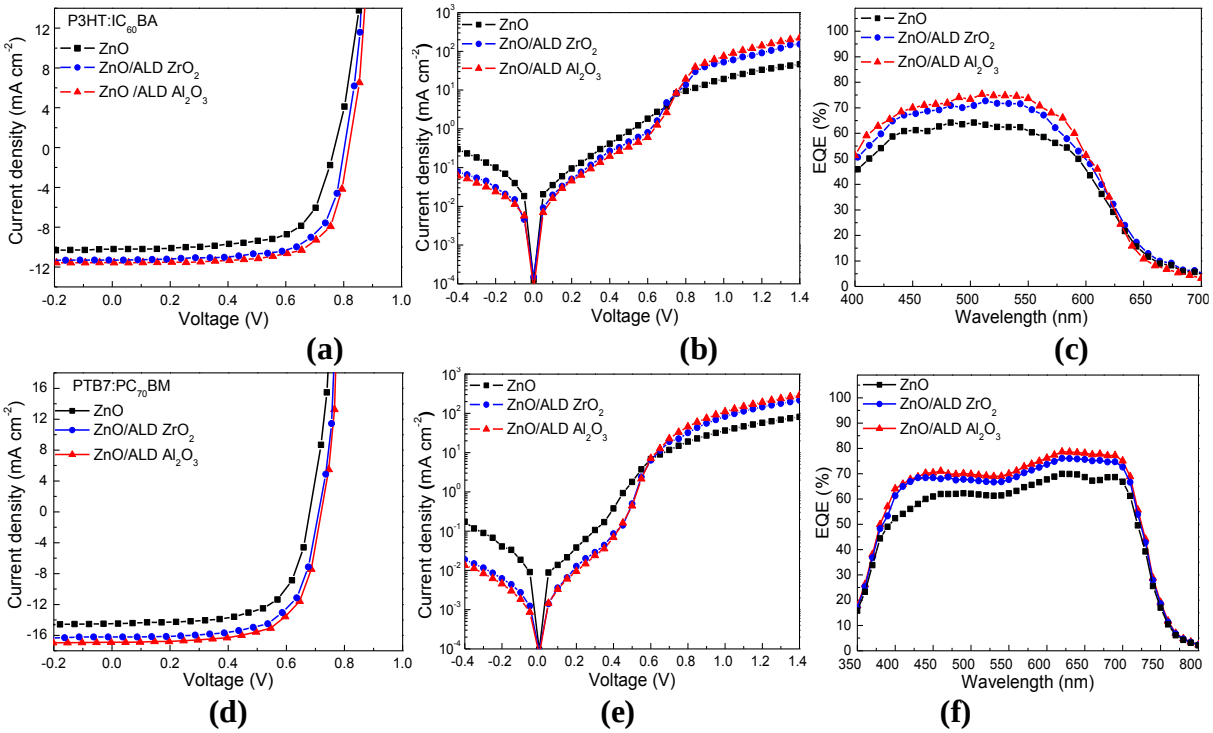

Figure 3 (a) Current density versus voltage (J-V) characteristics of P3HT:$IC_{60}BA$-based devices using un-passivated and ALD-dielectric coated ZnO films upon 1.5 AM illumination. (b) Dark J-V curves and (c) EQE measurements of the same devices. (d) J-V characteristics upon 1.5 AM illumination, (e) dark J-V curves and (f) EQE measurements of PTB7:$PC_{70}BM$-based devices using ZnO and ALD-dielectric coated ZnO EELs.

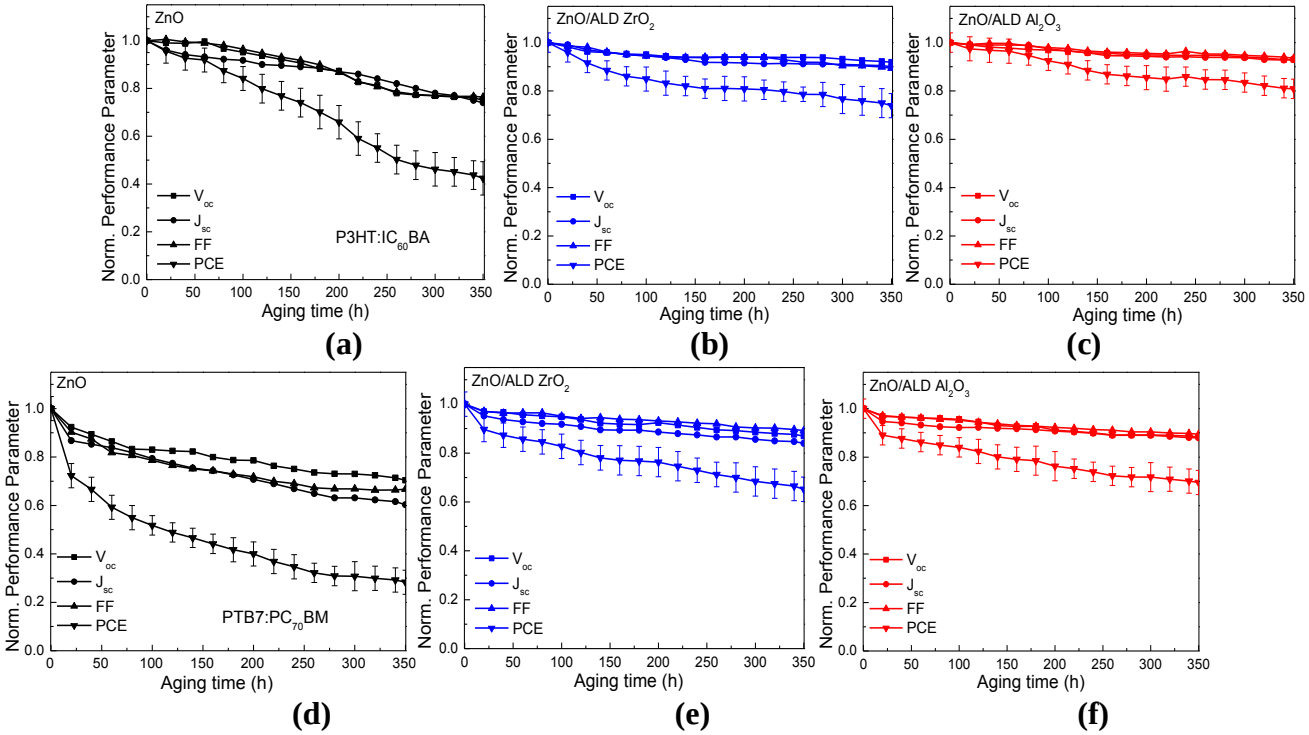

Figure 4 Stability measurements in ambient air: Variation of normalized PCE, J_{sc}, V_{oc} and FF over a period of 350 hours for P3HT:$IC_{60}BA$-based devices using (a) ZnO, (b) 6 cycles of ZrO_2 coated ZnO and (c) 6 cycles of Al_2O_3 coated ZnO layers and for PTB7:$PC_{70}BM$-based devices using (d) ZnO, (e) 6 cycles of ZrO_2 coated ZnO and (f) 6 cycles of Al_2O_3 coated ZnO layers. The error bars in PCEs are calculated as the standard deviation from the mean value for a set of 5 devices.

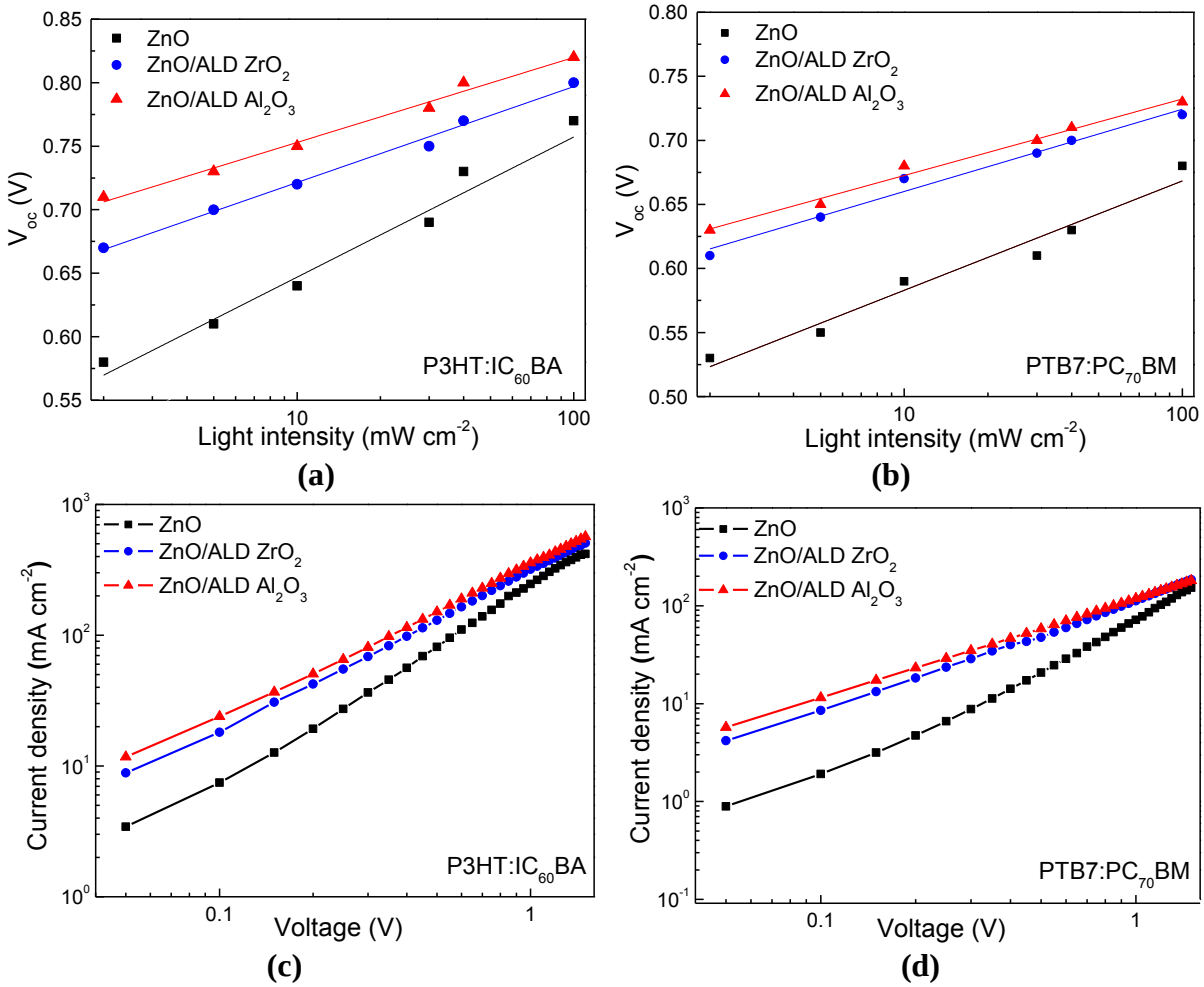

Figure 5 Dependence of V_{oc} on light intensity for (a) P3HT:$IC_{60}BA$-based and (b) PTB7:$PC_{70}BM$-based devices with un-passivated and ALD-dielectric coated ZnO layers. J–V curves in log-log plot obtained in electron-only (c) P3HT:$IC_{60}BA$-based and (d) PTB7:$PC_{70}BM$-based devices with un-passivated and ALD-dielectric coated ZnO layers measured in the dark.

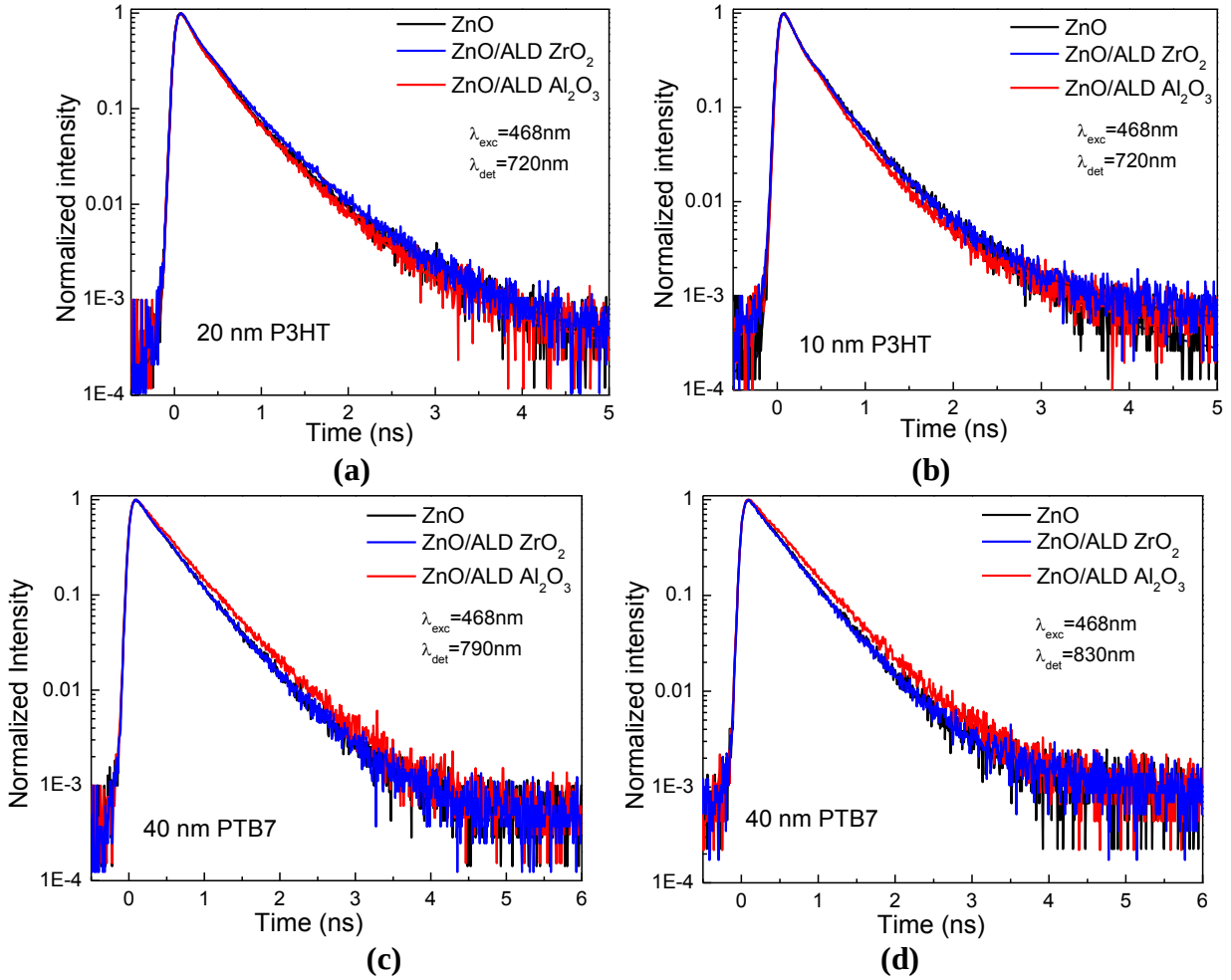

Figure 6 Normalized photoluminescence (PL) decay of (a) 20 nm thick P3HT and (b) 10 nm thick P3HT films deposited on un-passivated and ALD-dielectric coated ZnO layers, detected at 720 nm. PL decay of 40 nm thick PTB7 films deposited on un-passivated and ALD-dielectric-coated ZnO layers, detected at (c) 790 nm and (d) 830 nm, respectively.

Table 1 Photovoltaic parameters of solar cells with the configuration: glass substrate/FTO/ZnO or ALD-dielectric coated ZnO layer/active layer /MoO_x/Al (mean values and standard deviations were extracted from a set of 17 devices).

	J_{sc} (mA/cm^2)	V_{oc} (V)	FF	PCE (%)	R_s (Ω cm^2)	R_{sh} (Ω cm^2)
	P3HT:IC$_{60}$BA					
ZnO	10.20 (±0.10)	0.77 (±0.02)	0.64 (±0.01)	5.03 (±0.15)	4.3	2041
ZnO/ALD ZrO_2	11.30 (±0.10)	0.80 (±0.02)	0.69 (±0.01)	6.24 (±0.15)	3.0	2868
ZnO/ALD Al_2O_3	11.60 (±0.10)	0.82 (±0.02)	0.71 (±0.01)	6.75 (±0.15)	2.6	3498
	PTB7:PC$_{70}$BM					
ZnO	14.50 (±0.15)	0.68 (±0.02)	0.63 (±0.01)	6.21 (±0.20)	5.1	1825
ZnO/ALD ZrO_2	16.00 (±0.15)	0.71 (±0.02)	0.68 (±0.01)	7.72 (±0.20)	3.6	2639
ZnO/ALD Al_2O_3	16.80 (±0.15)	0.72 (±0.02)	0.68 (±0.01)	8.23 (±0.20)	3.4	2829